Published in final edited form as:
Dev Dyn. 2013 September ; 242(9): 1066–1077. doi:10.1002/dvdy.24000.

Region-specific Epithelial Cell Dynamics During Branching Morphogenesis

Jeff C. Hsu[2,1], **Hyun Koo**[2,3,1], **Jill S. Harunaga**[2,1], **Kazue Matsumoto**[2], **Andrew D. Doyle**[2,4], and **Kenneth M. Yamada**[2,4,*]

[2]Cell Biology Section, Laboratory of Cell and Developmental Biology, National Institute of Dental and Craniofacial Research, National Institutes of Health, Bethesda, MD

[3]Center for Oral Biology, University of Rochester Medical Center, Rochester, NY

Abstract

Background—Epithelial cells of developing embryonic organs, such as salivary glands, can display substantial motility during branching morphogenesis. Their dynamic movements and molecules involved in their migration are not fully characterized.

Results—We generated transgenic mice expressing photo-convertible KikGR and tracked the movements of individual cells highlighted by red fluorescence in different regions of developing salivary glands. Motility was highest for outer bud epithelial cells adjacent to the basement membrane, lower in inner bud cells, and lowest in duct cells. The highly motile outer cells contacting the basement membrane were pleomorphic, whereas inner cells were rounded. Peripheral cell motility was disrupted by antibodies inhibiting α6+β1 integrins and the non-muscle myosin II inhibitor blebbistatin. Inner bud cell migration was unaffected by these inhibitors, but their rate of migration was stimulated by inhibiting E-cadherin.

Conclusions—Cell motility in developing salivary glands was highest in cells in contact with the basement membrane. The basement membrane-associated motility of these outer bud cells depended on integrins and myosin II, but not E-cadherin. In contrast, motility of inner bud cells was restrained by E-cadherin. These findings identify the importance of integrin-dependent basement membrane association for the morphology, tissue organization, and lateral motility of morphogenetic epithelial cells.

Keywords

organ morphogenesis; salivary gland; cell migration; basement membrane; integrin; myosin II; E-cadherin; KikGR

[*]Correspondence to: K.M. Yamada, Laboratory of Cell and Developmental Biology, NIDCR, NIH, Bethesda, MD 20892, Tel: 301 496-9124, Fax: 301 402-0897, kenneth.yamada@nih.gov.
[1]J.C. Hsu, H. Koo, and J.S. Harunaga contributed equally to this work.
[4]A.D. Doyle and K.M. Yamada contributed equally to this work.

INTRODUCTION

Branching morphogenesis is a dynamic, complex process essential for embryonic development of multiple organs; it provides a mechanism for generating extensively branched but compact organs (reviewed in Lu and Werb, 2008; Affolter et al., 2009; Andrew and Ewald, 2010; Costantini and Kopan, 2010; Morrisey and Hogan, 2010; Kim and Nelson, 2012). The highly branched epithelial architecture of these organs generates large numbers of individual acini, alveoli, or other budlike structures that provide the large epithelial surface area needed for efficient secretion, gas exchange, or excretion. In mammals, organs that undergo branching morphogenesis include lungs, kidneys, and glands that include the salivary, mammary, and prostate glands.

In general, organ branching morphogenesis starts from a simple epithelial bud that undergoes repetitive branching while surrounded by a dense mesenchyme. Characteristic branching patterns occur for each organ, with a particularly stereotyped sequence of branching occurring during lung development (Metzger et al., 2008). Although some morphogenetic mechanisms may be shared, there appear to be differing strategies involving tube versus bud formation, as well as differing modes of branching or extension (Lu and Werb, 2008; Andrew and Ewald, 2010).

Beginning with the pioneering studies of Grobstein and colleagues on the regulation of branching morphogenesis (Grobstein, 1953; Grobstein and Cohen, 1965), mouse salivary gland development has been a classical model for understanding morphogenesis for more than a half-century. Murine salivary gland development involves complex three-dimensional branching and tissue remodeling (reviewed by (Melnick and Jaskoll, 2000; Kadoya and Yamashina, 2005; Patel et al., 2006; Tucker, 2007; Gresik et al., 2009; Andrew and Ewald, 2010; Hsu and Yamada, 2010; Larsen et al., 2010; Miletich, 2010; Sequeira et al., 2010; Harunaga et al., 2011).

Recent studies have revealed a surprisingly high degree of epithelial cell motility by individual cells or groups of cells during the early stages of branching morphogenesis of developing salivary glands (Larsen et al., 2006; Onodera et al., 2010) and other organs such as mammary glands (Ewald et al., 2008; Ewald et al., 2012) and *Drosophila* lungs (Metzger and Krasnow, 1999; Shakya et al., 2005). Epithelial cells of the kidney appear to have relatively modest levels of motility (Shakya et al., 2005), whereas the epithelial cells of salivary and mammary glands can show marked levels of migratory movement during branching morphogenesis (Larsen et al., 2006; Ewald et al., 2008). A number of growth factors such as HGF and FGF that are implicated in cell migration in other model developmental systems are expressed in developing glands, but their contribution to individual cell motility is not known (for example, see Larsen et al., 2010). These cell movements during branching morphogenesis have been suggested to contribute to the plasticity of tissues during the rapid architectural rearrangements of early organ formation.

There is, however, only limited information available about the patterns of movement of individual cells at different regions of developing mammalian organs. Developing salivary and mammary glands display extensive cell motility as characterized by time-lapse confocal

imaging (Larsen et al., 2006; Ewald et al., 2008). In developing mammary gland, the motility involves both collective and individual cell migration (Ewald et al., 2008; Ewald et al., 2012). In developing salivary glands, increased separation between individual cells located at the base of deepening clefts that delineate branching end buds is associated with a Btbd7 signaling pathway necessary for cleft formation (Onodera et al., 2010). The motion of GFP-labeled cells elsewhere in the developing salivary gland was visualized by infecting cells with a GFP-encoding adenovirus and appeared to be relatively random and autonomous (Larsen et al., 2006). Preliminary comparisons of movements of adenovirus-infected cells or cells moving out of a single optical plane suggest that the outer bud cells may be more motile (Larsen et al., 2006; Kadoya and Yamashina, 2010).

The epithelial cell motility that occurs transiently during salivary gland branching morphogenesis is developmentally regulated, and it ceases when glands mature to form the stable epithelial cell-cell adhesions characteristic of adult organisms (e.g., see Hieda et al., 1996; Larsen et al., 2006). In fact, the cell-cell adhesion complexes that comprise the classical adherens, tight, and desmosome-based junctions of very early epithelia are lost when oral epithelial cells undergo branching morphogenesis to form buds (Kadoya and Yamashina, 1993; Hieda et al., 1996). In developing mammary glands, adherens and tight junctions also appear to be lost during branching morphogenesis, although desmosomes remain (Ewald et al., 2012). These types of developmentally regulated, transient losses of cell-cell adhesive tissue integrity are likely to be important to permit rapid cell rearrangements and epithelial cell migratory movements.

Nevertheless, a number of major unanswered questions still remain concerning individual epithelial cell motility during branching morphogenesis. They include questions about whether there are systematic differences in rates and patterns of cell movement at different sites in developing organs, the relationship of cell motility to the basement membrane, and the roles of integrins, cadherins, and the actomyosin cytoskeleton in these embryonic epithelial cell movements.

RESULTS

Cell Highlighting System for Tracking Individual Cell Movements in 3D

Branching morphogenesis of the salivary gland is a highly dynamic process in which a single bud undergoes repetitive subdivision by clefts and branching to generate large numbers of buds (Movie 1). Although previous studies have used adenovirus infection of individual cells to track movements of salivary and mammary gland cells during this process of branching morphogenesis (Larsen et al., 2006; Ewald et al., 2012), it is not clear whether this approach might target only certain types of cells or could have subtle effects on cell migration. Consequently, we chose to use a transgenic mouse approach in which a fluorescent probe is expressed in all cells of an animal that undergoes normal embryonic development and organ morphogenesis. Instead of using a GFP derivative such as EGFP that labels every cell within a tissue such that it becomes impossible to track the migration of individual cells (Costantini et al. (2011) and unpublished results), we used the photo-convertible probe KikGR (Kikume green-red) generated by the Miyawaki laboratory (Tsutsui et al., 2005) to be able to distinguish between individual cells. KikGR is a green

fluorescent protein that can be converted to red fluorescence at local sites using low levels of 405 nm violet light, allowing us to identify motility patterns of individual cells without concerns about phototoxicity (e.g., see Fig. 1).

Ten independent transgenic mouse lines were generated after oocyte injection of the photo-convertible probe KikGR in a plasmid with *in vivo* expression driven by a CMV-actin promoter. We selected for subsequent studies a transgenic mouse line with the highest apparent expression of KikGR as determined by fluorescence microscopy. This line, named "KikGR," was maintained as a homozygous KikGR-expressing line that displayed cytoplasmic labeling of all tissues. Salivary glands from embryonic days (E)13–14 were maintained as three-dimensional organ explant cultures, which underwent efficient branching morphogenesis at rates indistinguishable from non-transgenic glands. The cells of these organs displayed green fluorescence except at sites of photo-conversion, for which we used a spot of 405 nm laser light directed by galvometric mirrors to photo-convert small groups of cells (Fig. 1B and 1C). This process generates a narrow column of photo-converted cells along the path of the laser light beam. Cell migration of these red-highlighted cells was compared between the three regions outlined diagrammatically in Fig. 1A: outer (peripheral) end bud cells located within 3–4 cell diameters of the basement membrane, inner bud cells from the central region of buds, and duct cells.

Individual cells marked by photoconversion showed no evidence of collective cell migration, but instead moved as independent single cells (Fig. 2A and Movie 2). The morphology of individual cells differed depending on their location within developing salivary glands. Static images show that the outer bud cells are more columnar than inner bud cells, with cells aligned adjacent to the epithelium-mesenchyme boundary (Fig. 3) (Walker et al., 2008). These partially columnar cells have cell widths of 5–8 μm and lengths of ~10 μm (J.S.H., unpublished results). However, live-cell imaging revealed that these outer bud cells were actually highly pleomorphic over time (Fig. 3B). They displayed rapid, major changes in cell shape when examined at 10-minute intervals, even while maintaining contact with the basement membrane (Fig. 3B and Movie 2). These substantial changes in cell morphology were not apparent by immunostaining of fixed samples, and they included rapid shortening or lengthening of the cell body with transient, local flattening of the leading edge as it contacted the basement membrane (Fig. 3). The inner bud cells tended to retain a more rounded morphology without the characteristic local flattening of outer bud cells touching the basement membrane (Fig. 3C and 3D).

Region-specific Differences in Velocity and Morphology during Epithelial Cell Migration

Migrating cells were monitored by time-lapse confocal spinning-disk microscopy, and the paths that they traversed were plotted and quantified by computer tracking using Volocity software (e.g., see Fig. 2B). Outer bud cells underwent significant motility, with an average velocity of 20±4 μm/hr (Fig. 4A). This rate of motility was substantially higher than in the two other regions (inner bud cell velocity 8±2 μm/hr and duct 5±1 μm/hr, $p<0.0001$ for both regions when compared to outer bud cell velocity). This difference was also reflected in the largest net displacement over a span of 160 minutes compared to the other two regions (Fig. 4B; $p<0.05$ for inner bud and $p<0.0001$ for duct). These outer cells often aligned along the

basal plasma membrane with E-cadherin localized at cell-cell junctions; however, E-cadherin localization was reduced at basal plasma membrane regions facing the basement membrane (Fig. 5A, white arrowheads). In contrast, the inner bud cells were more rounded and showed E-cadherin all around the cell periphery at cell-cell junctions (Fig. 5A). These morphological findings are consistent with published descriptions of partially columnar, aligned outer bud cells compared to the more rounded central bud cells (Walker et al., 2008; Onodera et al., 2010).

In time-lapse movies, these highly motile peripheral cells of the outer end bud displayed a particularly striking behavioral characteristic. These most-peripheral cells characteristically moved laterally with their leading edge in close proximity to the basement membrane, often appearing to nudge and bump along it in a manner reminiscent of fish swimming along an aquarium wall (Movie 2). The portion of these cells in direct contact with the basement membrane often spread out partially on this substrate, though cell shapes changed rapidly (Fig. 3B and Movie 2). In fact, polarity of such peripheral cells in direct contact with the basement membrane has been described previously (Daley et al., 2012). The outer bud cells periodically left the basement membrane and moved towards the bud interior accompanied by loss of their elongated, columnar shape, particularly when undergoing cell division (Movie 3). Such outer bud cells often returned quickly to the basement membrane, suggesting a stronger affinity for this matrix substrate compared to interactions with adjacent cells.

In contrast, the inner bud cells remained relatively rounded in shape with rates of motility approximately 2.5-fold lower in velocity than outer bud cells (Fig. 4A; $p<0.0001$). These inner bud cells rarely left the center of the bud to reach the basement membrane with quite limited intermixing of inner and outer bud cells in the time-lapse movies of photo-converted outer or inner bud regions (Fig. 2A, top panels, and Movie 4).

The epithelial cells located in ducts of developing glands were by far the least motile (Figs. 2 and 4). The differences in cell velocity between duct, inner bud, and outer bud cells were distinguishing characteristics, with little overlap in rates of migration between the epithelial cells from each region (Fig. 4A). Because cell motility by duct epithelial cells was so minimal, we focused our study on direct comparisons of the requirements for migration of the outer and inner bud epithelial cells.

Evaluation of Molecular Systems Involved in Morphogenetic Epithelial Cell Migration

Because time-lapse movies suggested that the outer bud epithelial cells often retained periodic contact with the basement membrane even while displaying substantial motility compared to adult epithelial cells, we tested whether integrin interactions were important for this behavior. Because interactions involving integrin α6 and β1 subunits with laminin and other components of basement membranes are important for salivary gland branching morphogenesis (Kadoya and Yamashina, 1993; Kadoya et al., 1998; Sakai et al., 2003; Kadoya and Yamashina, 2010), we inhibited this pair of integrin subunits with monoclonal antibodies. As previously reported, inhibiting integrin function inhibited gland branching morphogenesis (Fig. 5), but a particularly pertinent new finding was the morphological and functional effects on cell shape and motility. Integrin-inhibited cells lost all parallel

alignment along the basement membrane, and they abutted the basement membrane in relatively random patterns (Fig. 5B, right panels). Levels of E-cadherin were no longer low in basal plasma membrane regions facing the basement membrane, but instead E-cadherin was located around the entire cell periphery (Fig. 5B, red arrowheads), similar to the E-cadherin distribution for inner bud cells (Fig. 5A).

The velocity of motility of these outer bud cells after the addition of anti-integrin antibodies was inhibited more than 2-fold by this disruption of α6 and β1 integrin interactions (Fig. 6A, $p<0.001$). These cells no longer displayed their characteristic mode of motility involving nudging and bumping along the basement membrane, consistent with loss of basement membrane adhesion (Movies 5 and 6, and Fig. 6C). Their velocity after integrin inhibition became similar to that of control inner bud cells (compare Fig. 6A and 6B). Anti-β1 antibodies alone had substantially less effect on basement membrane association and cell motility (data not shown). Consistent with their absence of basement membrane interactions, the inner bud cells showed no change in velocity in response to this dual integrin inhibition (Fig. 6B). This finding also confirms that β1 integrins are not essential for inner bud cell motility, as predicted by the minimal amount of extracellular matrix within epithelial salivary end buds.

E-cadherin adhesive interactions are thought to be particularly important for inner bud cells destined to become duct cells later in development (Walker et al., 2008). In our short-term studies using live-cell imaging, inhibition of E-cadherin had no major effects on the organization of outer bud cells in terms of their characteristic semi-columnar organization and retention of E-cadherin localization at cell-cell junctions but not at regions facing the basement membrane. The outer epithelial cells remained associated with the basement membrane (Fig. 5C, yellow arrowheads), although they tended to appear variably less columnar and more disorganized. Outer bud cell motility and morphogenesis in general during the 20-hour analysis period were not significantly decreased after adding inhibitory anti-E-cadherin ECCD-1 monoclonal antibody ($p>0.05$). This latter finding indicates that cell-cell adhesion mediated by E-cadherin is not the mechanism mediating cell migration in contact with the basement membrane.

In contrast, inner bud cells showed a substantial, unexpected increase in migration rate after inhibition of E-cadherin (Fig. 6B, 60% elevation, $p<0.001$) during this 20-hour period, and the initially disparate rates of migration between outer and inner bud cells became indistinguishable after antibody inhibition of E-cadherin function (Fig. 6A, 6B, 16 μm/hr vs. 14 μm/hr, respectively, and Movies 7 and 8). This increase in inner bud cell migration velocity suggests that E-cadherin may act to suppress inner bud cell migration by stabilizing cell-cell interactions. In fact, intercellular spaces and holes become prominent shortly after anti-E-cadherin treatment, consistent with a loss of cell-to-cell adhesion permitting more-rapid individual cell motility. Interestingly, branching morphogenesis of the glands was not significantly affected until after 36 hours, when inhibitory E-cadherin antibody begins to substantially inhibit branching morphogenesis, with disruption of duct formation and cell death of inner bud cells as previously reported by Walker et al. (2008).

The role of non-muscle myosin II in cell migration on matrix substrates appears to differ when assayed *in vitro* on tissue culture substrates versus in three-dimensions, with negative versus positive roles in migration velocity, respectively depending on dimensionality of the matrix confronting migrating fibroblasts (see Discussion). We tested for the role of myosin II in 3D embryonic epithelial cell migration using blebbistatin to inhibit all myosin II isoforms. As previously described, blebbistatin reduced branching morphogenesis after ~4 hours (Daley et al., 2009) (and data not shown). Interestingly, inhibition of myosin II by blebbistatin had no effect on cell migration by inner bud cells for at least 15 hours, but it substantially reduced the rates of migration of outer bud cells by > 2-fold (Fig. 6A–C, $p<0.001$). This inhibition was accompanied by a modest reduction in the extent of columnar shape and cell organization, though cells tended to remain in close association with the basement membrane, similar to controls (compare Fig. 5A, white arrowheads with 5D, cyan arrowheads, and Movies 9 and 10). Consequently, the rapid 3D epithelial cell motility of outer bud cells is dependent on myosin II activity.

DISCUSSION

We used a combination of KikGR photo-conversion with quantitative analysis of 3D cell migration patterns to analyze the migration of single cells during branching morphogenesis. This approach identified region-specific patterns of migration involving differences in velocity, trajectory, and cell morphology; these patterns can alternatively depend on integrin-based interactions with the basement membrane, non-muscle myosin II, or E-cadherin, depending on the particular site. This approach to studying 3D single-cell motility using quantitative tracking analyses should be applicable to other developmental systems in order to identify quantitative requirements for specific molecules in the morphogenesis of branching organs.

Our conclusions from comparing individual epithelial cell migration patterns in different regions during salivary gland branching morphogenesis are that: (a) photo-conversion of a KikGR marker permits tracking of the morphology and motility of individual cells in an explanted organ undergoing morphogenesis without the need for viral infection; (b) even though static images show that the epithelial cells immediately adjacent to the basement membrane of salivary glands undergoing branching morphogenesis are relatively organized in a semi-columnar pattern compared to cells at the interior of end buds, these outer bud cells undergo rapid, extensive changes in shape and location; (c) the motility of outer bud cells is the highest of all the epithelial cells in these developing glands in the order of velocities: outer bud > inner bud > duct; (d) even though they have the highest motility, outer cells tend to remain in close proximity to the basement membrane; (e) disrupting integrin-mediated cell interactions with the basement membrane disrupts the motility of these outer bud cells, which become more rounded and less organized in terms of parallel alignment; (f) 3D migration of outer bud cells is also dependent on myosin II activity, which is opposite to reported findings for cells in 2D regular culture surfaces; (g) migration of outer bud cells was not substantially affected by disruption of E-cadherin function; and (h) migration of inner bud cells was significantly increased by inhibition of E-cadherin, indicating that it is inversely dependent on this cell-cell adhesion molecule, which actually acts to restrain rates of inner bud cell migration.

In embryonic salivary glands, the outer bud epithelial cells adjacent to the basement membrane are known to be morphologically distinct, with differences in ultimate differentiated cell fate compared to the inner bud cells (Walker et al., 2008). The outer, peripheral cells are more columnar than cells in the interior, and they display more organized cell-cell junctions containing the cell-cell adhesion molecule E-cadherin. Specifically, the outer bud cells express the B1 antigen marker characteristic of more mature acini, and were reported to become acini rather than ducts as development proceeds; in contrast, the inner bud cells are destined to become secondary ducts (Walker et al., 2008).

Even though the outer bud cells appear more organized at the tissue level, our study revealed unexpectedly that they are substantially more motile than inner bud and duct cells, and they are also highly pleomorphic. These cells at the bud periphery frequently contacted the basement membrane, either migrating along it or touching, leaving, and returning. Inhibition of the integrins thought to mediate cell interactions with basement membranes reduced their migration speed to that of inner bud cells, with a loss of their characteristic quasi-columnar organization. In marked contrast, the rate of motility of the inner buds cells was unaffected by the same integrin inhibition, consistent with the minimal amount of extracellular matrix proteins in this region of the developing salivary gland. These findings identify a central role for epithelial cell-basement membrane interactions in salivary gland cell motility patterns. We speculate that the high level of motility and plasticity of cell shape is a prerequisite for the subsequent step of ingression of cells at the tip of the end bud to form a cleft. Our study also confirms the importance of these integrin interactions for cleft progression and bud formation, which involves subsequent local expression of Btbd7, cell separation to form gaps, and gradual cleft progression (Onodera et al., 2010).

Our findings concerning the importance of cell-basement membrane interactions are consistent with previous studies establishing the importance of the basement membrane components collagen (which we suggest includes collagen IV in the basement membrane besides collagens I or III associated with mesenchyme), proteoglycans, laminin, and fibronectin in salivary gland branching morphogenesis (Grobstein and Cohen, 1965; Bernfield et al., 1972; Kadoya et al., 1998; Sakai et al., 2003). Disrupting cell interactions with the basement membrane by anti-integrin antibodies switched the morphology, migration rate, and E-cadherin localization pattern of the outer bud cells to a pattern characteristic of inner bud cells. Consequently, we propose that a crucial contributor to the previously described distinct morphology and markers of the outer, periphery bud cells (Walker et al., 2008; Onodera et al., 2010) is the dynamic integrin-mediated interaction of these cells with the basement membrane. This integrin interaction also plays a key role in maintaining the high rate and basement membrane-hugging mode of epithelial cell migration and the overall process of branching morphogenesis.

The role of non-muscle myosin II that we observe in rapid cell migration of outer bud cells in three-dimensional organ development differs from observations for cell migration on matrix substrates *in vitro* on tissue culture substrates. In two-dimensional cell culture, inhibiting myosin II with blebbistatin or by gene ablation or knockdown generally results in increased lamellipodial protrusive activity and accelerated migration of both fibroblasts and epithelial cells from a morphogenetic tissue (Even-Ram et al., 2007; Vicente-Manzanares et

al., 2007; Pasapera et al., 2010; Plosa et al., 2012), whereas cell migration was inhibited within developing glands in this study, as well as in studies of cells migrating in three-dimensional *in vitro* cell culture systems (Nakayama et al., 2005; Wilkinson et al., 2005; Doyle et al., 2009; Derycke et al., 2011; Petrie et al., 2012). Thus, myosin II appears to play a role as a brake on rates of migration in 2D conditions by promoting cell-matrix adhesion formation. In contrast, it is required for efficient migration by the outer epithelial cells in 3D. Although inhibition of myosin II isoforms by blebbistatin can initially increase the numbers of clefts and branches in developing salivary gland and lung (Daley et al., 2009; Plosa et al., 2012), it ultimately inhibits cleft progression and branching. Besides inhibiting 3D epithelial migration as shown in this study, the loss of contractility inhibits the process of fibronectin matrix assembly known to be necessary for ongoing salivary gland branching morphogenesis (Sakai et al., 2003; Daley et al., 2009).

It is important to note that there are at least two distinct modes of 3D migration identified in this study: cell migration associated with the basement membrane and cell migration in the inner bud where there are minimal matrix proteins. As discussed above, integrins and myosin II are needed for efficient migration of the outer bud cells. The inner bud cells migrate more slowly, and interestingly, their migration is not dependent on either of these integrin and myosin II contributors to rapid outer bud cell migration. Moreover, the migration of outer bud cells and branching morphogenesis are minimally affected by inhibition of E-cadherin for at least 20 hours, whereas inner bud cell motility is much more sensitive. Importantly, however, that sensitivity involves a 60% acceleration of migration, indicating that the speed of inner bud epithelial cells is actually being restrained by E-cadherin interactions. These E-cadherin adhesive interactions may normally act to hold inner bud cells at the center of the bud, reducing their intermixing with outer bud cells. This contribution to segregation of cell types could help maintain differences in fate, i.e., ductal versus acinar (Walker et al., 2008).

In summary, tracking of individual cell migration at different sites of an organ undergoing branching morphogenesis has revealed region-specific migration rates and differences in dependence on molecular contributors or inhibitors of migration. A key concept identified in this study is the central role of epithelial cell-basement membrane interactions in the rapid epithelial cell migration of outer end bud cells; they contribute to the distinctive dynamic cell morphology and migration of these cells compared to inner bud cells. In addition, roles of myosin II and E-cadherin differ in these two regions of buds, consistent with the concept of region-specific differences in cell-matrix interactions, cell motility, and cell fate within epithelial end buds contributing to different aspects of branching morphogenesis.

EXPERIMENTAL PROCEDURES

Generation of KikGR pCLE Plasmid and Transgenic Mice

KikGR (Kikume green-red) is a green fluorescent protein (excitation 510 nm, emission 517 nm) that can be photoconverted using low levels of violet light (excitation 405 nm) to red fluorescence (excitation 583 nm, emission 593 nm). A plasmid containing the KikGR coding sequence, pCS2+KikGR, and pCLE GFP were kind gifts from Dr. Atsushi Miyawaki (RIKEN) and Dr. Andrzej Dlugosz (University of Michigan), respectively (Tsutsui et al.,

2005; Bradley et al., 2007). KikGR and a Kozak sequence flanked by NotI and NheI sites were amplified by PCR using the 5' primer GCGGCCGCCACCATGGTGAGTGTGATTACATCAGAAATGAAGATCGAGCTG and 3' primer GCTAGCTTACTTGGCCAGCCTTGGCAGCCCGGAATGAGC. The KikGR fragment was inserted into NotI and NheI sites of pCLE GFP. The GFP sequence was excised by recombineering (Warming et al., 2005) using SW 106 cells (Mouse Cancer Genetics Program, NCI, Frederick). The GFP-excised clone was retransformed into DH5α (Invitrogen), and deletion of GFP was confirmed by KpnI digestion. The KikGR coding sequence was verified by sequencing. The entire insert with promoter and KikGR sequence was excised with KpnI and gel-purified for microinjection into fertilized FVB mouse oocytes. KikGR-expressing transgenic mice were generated as described by (Cho et al., 2009) and genotyped by PCR using 5' primers CTCTAGAGCCTCTGCTAACC or GTGAGTGTGATTACATCAGAAATG with 3' primer CCTCAGGAAACGACTGCTTGAAG. All animal procedures were approved by the NIDCR Animal Care and Use Committee.

Salivary Gland Dissection and Organ Culture

Timed pregnant KikGR mice were euthanized on embryonic day 13 (E13, 13 days after finding a vaginal plug). The submandibular salivary glands (SMG) were dissected out and cultured overnight on a membrane filter (Whatman Nuclepore track-etch polycarbonate membranes, 13 mm, 0.2 μm pore size) floating on DMEM/F12 medium (Invitrogen) supplemented with 100 U/ml penicillin, 100 μg/ml streptomycin, 150 μg/ml ascorbic acid and 50 μg/ml transferrin. After overnight culture, the filter was flipped over so the SMG faced downward and was attached with vacuum grease (Dow Corning) to a glass bottom dish (MatTek Corp). Standard media as described above plus OxyFluor (Oxyrase), 2.5 μg/ml 647-labelled (see procedure below) collagen IV antibody (Millipore) was then added. For inhibitory experiments, 100 μg/ml ECCD-1 function-blocking E-cadherin antibody (Invitrogen), 50 μM blebbistatin (Calbiochem), or a combination of 100 μg/ml GoH3 anti-α6 integrin and 100 μg/ml Ha1/2 anti-β1 integrin (BD Pharmingen) were included in the media. The glands were allowed to incubate for approximately 5–8 hours before imaging up to 20 hours after the addition of inhibitors. For blebbistatin treatment, cells were first photoconverted, then this inhibitor was added immediately prior to imaging; for all other experiments, treatment was initiated immediately after affixing the glands to the glass-bottom dish.

Labeling of Collagen IV antibodies

Collagen IV antibodies were first concentrated to >1.5mg/ml prior to the addition of a 7-fold molar excess of Alexa Fluor 647 NHS-ester dye (Invitrogen, Eugene, OR) solubilized in DMSO (Sigma-Aldrich, St Louis, MO). The antibody-dye mixture was gently rotated at 4°C for 2 hours. Excess dye was removed with buffer exchange columns (Pierce, Rockford, IL) against PBS (HyClone, Logan UT).

Spinning Disk Microscopy and KikGR Photoconversion

For 3D time-lapse imaging of KIKGR SMGs, we used a CSU-X1 spinning disk confocal (Yokogawa, Tokyo, Japan) attached to a Zeiss Axiovert 200M microscope using a 20× Plan-

Apochromat objective (NA 0.8) or a S-Apochromat silicone oil (NA 1.15) immersion objective (Olympus, Center Valley, PA). An LMM5 laser merge module (Spectral Applied Research, Ontario, Canada) equipped with 405 nm (100 mW), 488 nm (100 mW), 561(50 mW) and 642 nm (100 mW) diode lasers provided excitation wavelengths. The primary dichroic (405/488/561/640) and accompanying emission filters were from Semrock (Rochester, NY). Images were captured at 14-bits using a 512 backthinned EM CCD camera (Hamamatsu, NJ). X, Y, and Z positioning was performed by a MS-2000 Z-piezo stage from ASI (Eugene, OR). An environmental chamber on the microscope maintained at a constant temperature of 37°C with constant CO2 and humidity. All components were controlled with MetaMorph imaging software (Molecular Devices, Downington, PA).

Images for each emission channel were acquired over a total Z-section of 20 μm (Z-spacing of 2 μm) every 10 minutes for up to 12 hours. SMG were imaged with 488 nm, 561 nm and 642 nm excitation wavelengths, except for experiments with blebbistatin where only 561 nm and 642 nm excitation lines with used. Prior to photoconversion, SMGs were bleached with 100% 561 nm laser light for 20 seconds to reduce background noise. Exposure times for each channel were set to between 300–600 msec depending on brightness. Laser power settings were set to 12%, 18%, and 8%, for 488 nm, 561 nm, and 642 nm excitation lines, respectively.

For photo-conversion, an iLAS FRAP module (Roper Scientific Europe, France) was used together with a 50 mW 405 nm diode laser (CrystaLaser, Reno, NV). The “FRAP on the fly” module was used with an 8 pixel diameter with an output power of 20%. Cells were photo-converted until 561 nm images demonstrated a large dynamic range at 14-bits, with the average light exposure being between 10–20 sec. This photo-conversion method using a focused beam of laser illumination resulted in multiple cells being photo-converted in a column, with the Z-section height dependent on the numerical aperture of the objective. It should be noted that attempts were made to photo-convert cells using two-photon excitation as previously indicated (Tsutsui et al., 2005), but we were unable to photo-convert cells sufficiently robustly even after testing multiple wavelengths with multiple approaches. The 405 nm laser provided the best conversion source. For multi-position imaging of up to 18 positions and 16 glands, 3 to 4 glands were placed in each well of a 6-well MatTek dish.

Image Filtering and Analysis

Prior to 3D cell tracking, each 561 nm time point was filtered several times to reduce background noise and smooth edges using MetaMorph. All filtering was performed at each single Z-slice. The filtering is as follows: 1) Background flattening of objects below 18 pixels in diameter, 2) 5×5 Gaussian filter, 3) 9×9 unsharp mask, 4) 3×3 low pass, 5) 5×5 Gaussian filter, 6) 3×3 low pass, 7) 5×5 Gaussian filter (See Fig. 7 for a depiction of the process and the filter kernels). For generating isosurface and orthogonal images, unfiltered data were processed by deconvolution using AutoQuant software (MediaCybernetics, Bethesda, MD), using the AutoQuant adaptive point spread function. Images for isosurfacing were then imported into Imaris 7.4 (Bitplane AG Zurich, Switzerland).

Tracking of Cell Migration

Single cells were tracked using 3D image recognition and image analysis software Volocity® (Perkin Elmer, Inc.), with position (X, Y, and Z) measurements every 10 min. Briefly, pre-filtered images were imported into Volocity® and individual cells were found using intensity-based thresholding and then either excluded or retained based upon fluorescence and size. The software based object (cell) recognition was confirmed by visual observation of Volocity® data images by an experienced user as detailed elsewhere (Piltti et al., 2011). Cells that (a) could not be tracked for the full time period, (b) were too close to each other, or (c) dividing were excluded from analysis. Cells were tracked for 160 minutes (17 frames) using the Volocity® automated cell-centroid tracking algorithm. Each of the software-generated tracks was checked independently by two individuals at the single-frame level to confirm that the tracks agreed with visual observation. All cell tracks were quantified for velocity (μm/hr) and net displacement (μm). For visualization, tracks of migrating cells from a representing experiment were displayed as 3D plots (X, Y, Z axis).

Immunofluorescence Staining

Intact submandibular salivary glands were fixed with 4% paraformaldehyde and immunostained as described previously (Onodera et al., 2010) using primary antibodies as indicated with species-specific donkey anti-IgG Cy2 and Cy3-labeled secondary antibodies from Jackson ImmunoResearch. Images were acquired with a Zeiss 710 laser scanning confocal microscope using a 40× (1.3 NA) Plan Apochromat oil immersion objective (Zeiss, Thornwood, NY). 488 nm argon and 543 nm HeNe lasers were used to excite Cy2 and Cy3 fluorophores, respectively. The pinholes for each laser line were aligned for optimal confocality. Images were processed with using a low pass filter (3×3 pixels) using MetaMorph, then brightness and contrast were adjusted using Adobe Photoshop software.

Supplementary Material

Refer to Web version on PubMed Central for supplementary material.

Acknowledgments

We thank Dr. Atsushi Miyawaki for the KikGR photo-convertible fluorescence probe and for advice, Dr. Kenn Holmbeck for advice on recombineering, Dr. Andrzej Dlugosz for the pCLE GFP plasmid, and Andrew Cho, Bradford Hall, Ashok Kulkarni, and the NIDCR Gene Targeting Core for generating KikGR transgenic mouse lines. Supported by the Intramural Research Program of the National Institute of Dental and Craniofacial Research, National Institutes of Health.

REFERENCES

Affolter M, Zeller R, Caussinus E. Tissue remodelling through branching morphogenesis. Nat Rev Mol Cell Biol. 2009; 10:831–842. [PubMed: 19888266]

Andrew DJ, Ewald AJ. Morphogenesis of epithelial tubes: Insights into tube formation, elongation, and elaboration. Dev Biol. 2010; 341:34–55. [PubMed: 19778532]

Bernfield MR, Banerjee SD, Cohn RH. Dependence of salivary epithelial morphology and branching morphogenesis upon acid mucopolysaccharide-protein (proteoglycan) at the epithelial surface. J Cell Biol. 1972; 52:674–689. [PubMed: 4109690]

Bradley SV, Hyun TS, Oravecz-Wilson KI, Li L, Waldorff EI, Ermilov AN, Goldstein SA, Zhang CX, Drubin DG, Varela K, Parlow A, Dlugosz AA, Ross TS. Degenerative phenotypes caused by the

combined deficiency of murine HIP1 and HIP1r are rescued by human HIP1. Hum Mol Genet. 2007; 16:1279–1292. [PubMed: 17452370]

Cho A, Haruyama N, Kulkarni AB. Generation of transgenic mice. Curr Protoc Cell Biol Chapter. 2009; 19(Unit 19):11.

Costantini F, Kopan R. Patterning a complex organ: branching morphogenesis and nephron segmentation in kidney development. Dev Cell. 2010; 18:698–712. [PubMed: 20493806]

Costantini F, Watanabe T, Lu B, Chi X, Srinivas S. Imaging kidney development. Cold Spring Harb Protoc. 2011; 2011 pdb top109.

Daley WP, Gervais EM, Centanni SW, Gulfo KM, Nelson DA, Larsen M. ROCK1-directed basement membrane positioning coordinates epithelial tissue polarity. Development. 2012; 139:411–412. [PubMed: 22186730]

Daley WP, Gulfo KM, Sequeira SJ, Larsen M. Identification of a mechanochemical checkpoint and negative feedback loop regulating branching morphogenesis. Dev Biol. 2009; 336:169–182. [PubMed: 19804774]

Derycke L, Stove C, Vercoutter-Edouart AS, De Wever O, Dolle L, Colpaert N, Depypere H, Michalski JC, Bracke M. The role of non-muscle myosin IIA in aggregation and invasion of human MCF-7 breast cancer cells. Int J Dev Biol. 2011; 55:835–840. [PubMed: 22161839]

Doyle AD, Wang FW, Matsumoto K, Yamada KM. One-dimensional topography underlies three-dimensional fibrillar cell migration. J Cell Biol. 2009; 184:481–490. [PubMed: 19221195]

Even-Ram S, Doyle AD, Conti MA, Matsumoto K, Adelstein RS, Yamada KM. Myosin IIA regulates cell motility and actomyosin-microtubule crosstalk. Nat Cell Biol. 2007; 9:299–309. [PubMed: 17310241]

Ewald AJ, Brenot A, Duong M, Chan BS, Werb Z. Collective epithelial migration and cell rearrangements drive mammary branching morphogenesis. Dev Cell. 2008; 14:570–581. [PubMed: 18410732]

Ewald AJ, Huebner RJ, Palsdottir H, Lee JK, Perez MJ, Jorgens DM, Tauscher AN, Cheung KJ, Werb Z, Auer M. Mammary collective cell migration involves transient loss of epithelial features and individual cell migration within the epithelium. J Cell Sci. 2012; 125:2638–2654. [PubMed: 22344263]

Gresik EW, Koyama N, Hayashi T, Kashimata M. Branching morphogenesis in the fetal mouse submandibular gland is codependent on growth factors and extracellular matrix. J Med Invest. 2009; 56(Suppl):228–233. [PubMed: 20224186]

Grobstein C. Morphogenetic interaction between embryonic mouse tissues separated by a membrane filter. Nature. 1953; 172:869–870. [PubMed: 13111219]

Grobstein C, Cohen J. Collagenase: effect on the morphogenesis of embryonic salivary epithelium in vitro. Science. 1965; 150:626–628. [PubMed: 5837103]

Harunaga J, Hsu JC, Yamada KM. Dynamics of salivary gland morphogenesis. J Dent Res. 2011; 90:1070–1077. [PubMed: 21487116]

Hieda Y, Iwai K, Morita T, Nakanishi Y. Mouse embryonic submandibular gland epithelium loses its tissue integrity during early branching morphogenesis. Dev Dyn. 1996; 207:395–403. [PubMed: 8950514]

Hsu JC, Yamada KM. Salivary gland branching morphogenesis--recent progress and future opportunities. Int J Oral Sci. 2010; 2:117–126. [PubMed: 21125789]

Kadoya Y, Nomizu M, Sorokin LM, Yamashina S, Yamada Y. Laminin alpha1 chain G domain peptide, RKRLQVQLSIRT, inhibits epithelial branching morphogenesis of cultured embryonic mouse submandibular gland. Dev Dyn. 1998; 212:394–402. [PubMed: 9671943]

Kadoya Y, Yamashina S. Distribution of alpha 6 integrin subunit in developing mouse submandibular gland. J Histochem Cytochem. 1993; 41:1707–1714. [PubMed: 8409377]

Kadoya Y, Yamashina S. Salivary gland morphogenesis and basement membranes. Anat Sci Int. 2005; 80:71–79. [PubMed: 15960312]

Kadoya Y, Yamashina S. Cellular dynamics of epithelial clefting during branching morphogenesis of the mouse submandibular gland. Dev Dyn. 2010; 239:1739–1747. [PubMed: 20503369]

Kim HY, Nelson CM. Extracellular matrix and cytoskeletal dynamics during branching morphogenesis. Organogenesis. 2012; 8:56–64. [PubMed: 22609561]

Larsen M, Wei C, Yamada KM. Cell and fibronectin dynamics during branching morphogenesis. J Cell Sci. 2006; 119:3376–3384. [PubMed: 16882689]

Larsen M, Yamada KM, Musselmann K. Systems analysis of salivary gland development and disease. Wiley Interdisciplinary Reviews: Systems Biology and Medicine. 2010 http://wires.wiley.com/WileyCDA/WiresArticle/wisId-WSBM94.html.

Lu P, Werb Z. Patterning mechanisms of branched organs. Science. 2008; 322:1506–1509. [PubMed: 19056977]

Melnick M, Jaskoll T. Mouse submandibular gland morphogenesis: a paradigm for embryonic signal processing. Crit Rev Oral Biol Med. 2000; 11:199–215. [PubMed: 12002815]

Metzger RJ, Klein OD, Martin GR, Krasnow MA. The branching programme of mouse lung development. Nature. 2008; 453:745–750. [PubMed: 18463632]

Metzger RJ, Krasnow MA. Genetic control of branching morphogenesis. Science. 1999; 284:1635–1639. [PubMed: 10383344]

Miletich I. Introduction to salivary glands: structure, function and embryonic development. Front Oral Biol. 2010; 14:1–20. [PubMed: 20428008]

Morrisey EE, Hogan BL. Preparing for the first breath: genetic and cellular mechanisms in lung development. Dev Cell. 2010; 18:8–23. [PubMed: 20152174]

Nakayama M, Amano M, Katsumi A, Kaneko T, Kawabata S, Takefuji M, Kaibuchi K. Rho-kinase and myosin II activities are required for cell type and environment specific migration. Genes Cells. 2005; 10:107–117. [PubMed: 15676022]

Onodera T, Sakai T, Hsu JC, Matsumoto K, Chiorini JA, Yamada KM. Btbd7 regulates epithelial cell dynamics and branching morphogenesis. Science. 2010; 329:562–565. [PubMed: 20671187]

Pasapera AM, Schneider IC, Rericha E, Schlaepfer DD, Waterman CM. Myosin II activity regulates vinculin recruitment to focal adhesions through FAK-mediated paxillin phosphorylation. J Cell Biol. 2010; 188:877–890. [PubMed: 20308429]

Patel VN, Rebustini IT, Hoffman MP. Salivary gland branching morphogenesis. Differentiation. 2006; 74:349–364. [PubMed: 16916374]

Petrie RJ, Gavara N, Chadwick RS, Yamada KM. Nonpolarized signaling reveals two distinct modes of 3D cell migration. J Cell Biol. 2012; 197:439–455. [PubMed: 22547408]

Plosa EJ, Gooding KA, Zent R, Prince LS. Nonmuscle myosin II regulation of lung epithelial morphology. Dev Dyn. 2012; 241:1770–1781. [PubMed: 22972683]

Sakai T, Larsen M, Yamada KM. Fibronectin requirement in branching morphogenesis. Nature. 2003; 423:876–881. [PubMed: 12815434]

Sequeira SJ, Larsen M, DeVine T. Extracellular matrix and growth factors in salivary gland development. Front Oral Biol. 2010; 14:48–77. [PubMed: 20428011]

Shakya R, Watanabe T, Costantini F. The role of GDNF/Ret signaling in ureteric bud cell fate and branching morphogenesis. Dev Cell. 2005; 8:65–74. [PubMed: 15621530]

Tsutsui H, Karasawa S, Shimizu H, Nukina N, Miyawaki A. Semi-rational engineering of a coral fluorescent protein into an efficient highlighter. EMBO Rep. 2005; 6:233–238. [PubMed: 15731765]

Tucker AS. Salivary gland development. Semin Cell Dev Biol. 2007; 18:237–244. [PubMed: 17336109]

Vicente-Manzanares M, Zareno J, Whitmore L, Choi CK, Horwitz AF. Regulation of protrusion, adhesion dynamics, and polarity by myosins IIA and IIB in migrating cells. J Cell Biol. 2007; 176:573–580. [PubMed: 17312025]

Walker JL, Menko AS, Khalil S, Rebustini I, Hoffman MP, Kreidberg JA, Kukuruzinska MA. Diverse roles of E-cadherin in the morphogenesis of the submandibular gland: insights into the formation of acinar and ductal structures. Dev Dyn. 2008; 237:3128–3141. [PubMed: 18816447]

Warming S, Costantino N, Court DL, Jenkins NA, Copeland NG. Simple and highly efficient BAC recombineering using galK selection. Nucleic Acids Res. 2005; 33:e36. [PubMed: 15731329]

Wilkinson S, Paterson HF, Marshall CJ. Cdc42-MRCK and Rho-ROCK signalling cooperate in myosin phosphorylation and cell invasion. Nat Cell Biol. 2005; 7:255–261. [PubMed: 15723050]

Key findings

- Motility of individual salivary gland epithelial cells differs by region during branching morphogenesis.
- Migration speed is highest in outer bud cells close to the basement membrane and low in inner bud and duct cells.
- Integrin interactions are necessary for both motility and morphology of outer bud cells.
- Myosin II, but not E-cadherin, is needed for outer bud cell migration.
- These findings identify crucial roles for epithelial cell interactions with the basement membrane for both high motility and tissue organization.

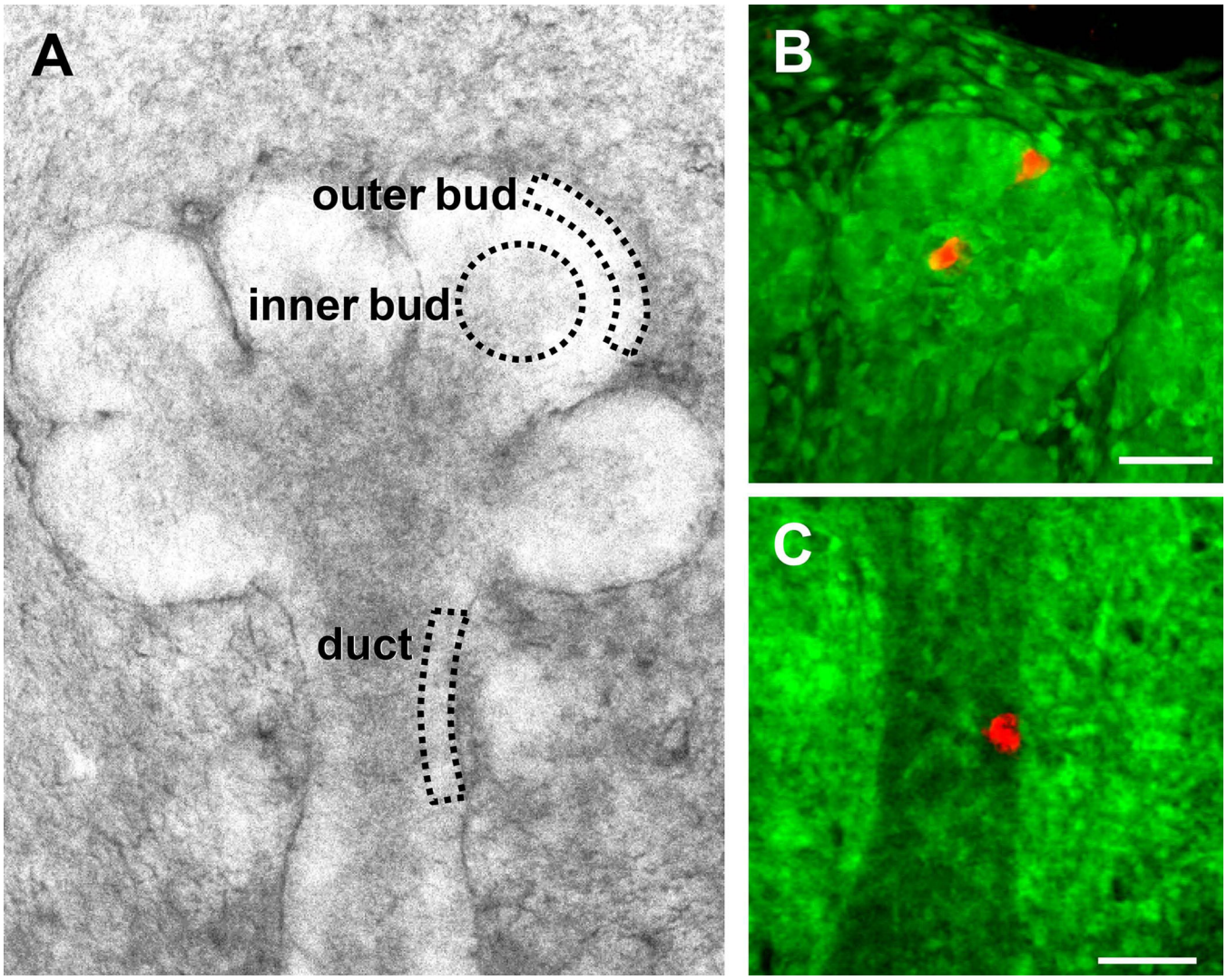

Fig. 1.

Region-specific fluorescence cell highlighting to track migration of individual epithelial cells during morphogenesis. **A:** E13.5 submandibular salivary gland in 3D organ explant culture indicating the three epithelial regions being compared in this study. The outer bud region highlighted cells at the apex of the bud located away from clefts, and the inner bud region characterized cells located more centrally in the bud. **B,C:** A focused, narrow beam of 405 nm laser light was used to photo-convert KikGR fluorescence from green to red in end bud inner or outer regions (B) or duct (C). A single region estimated to contain at least 8–10 cells was photo-converted immediately prior to initiating the imaging for panels B and C. For clarity, these images are maximum intensity projections of Z-slices for the red channel and a single Z-slice for the green channel. Bars, 50 μm.

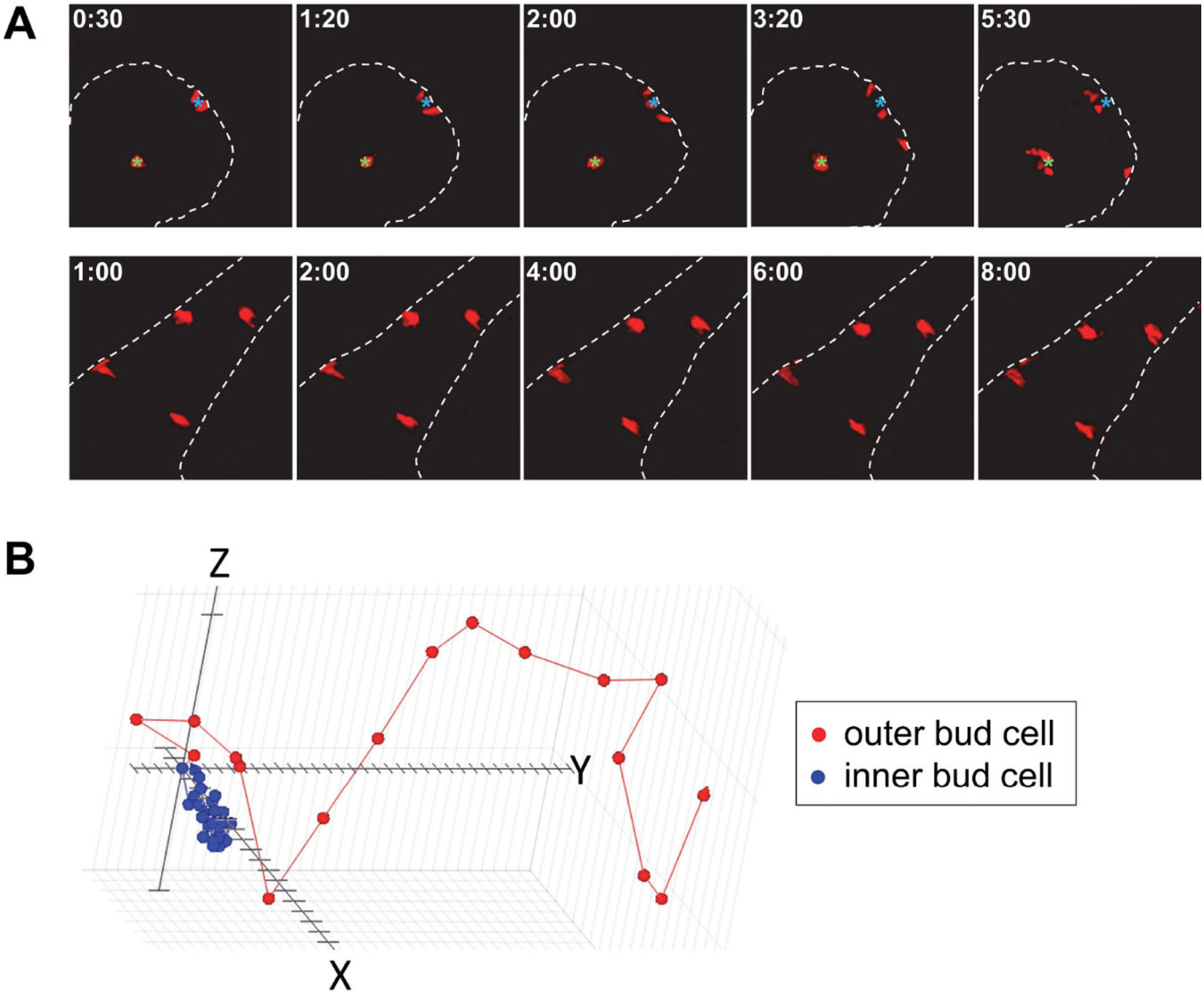

Fig. 2.

Representative examples of photoconverted KikGR cells undergoing migration as visualized by time-lapse spinning disk confocal microscopy. **A:** Time-lapse series illustrating the region-specific migration of outer and inner bud cells (upper panels) and duct cells (lower panels); the images are 20 μm maximum intensity Z projections. Note the higher rate of lateral cell motility of the outer bud cells along the basement membrane (dotted line). In contrast, the duct epithelial cells show virtually no migration. Green and cyan fiduciary marks denote the original position of the cells in the inner and outer bud region, respectively. **B:** Representative automated 3D computer tracking of an outer (red) and an inner (blue) bud cell using Volocity software; the distance between tick marks on the X, Y, and Z axes is 2.5 μm, with the consecutive points representing 10-minute intervals.

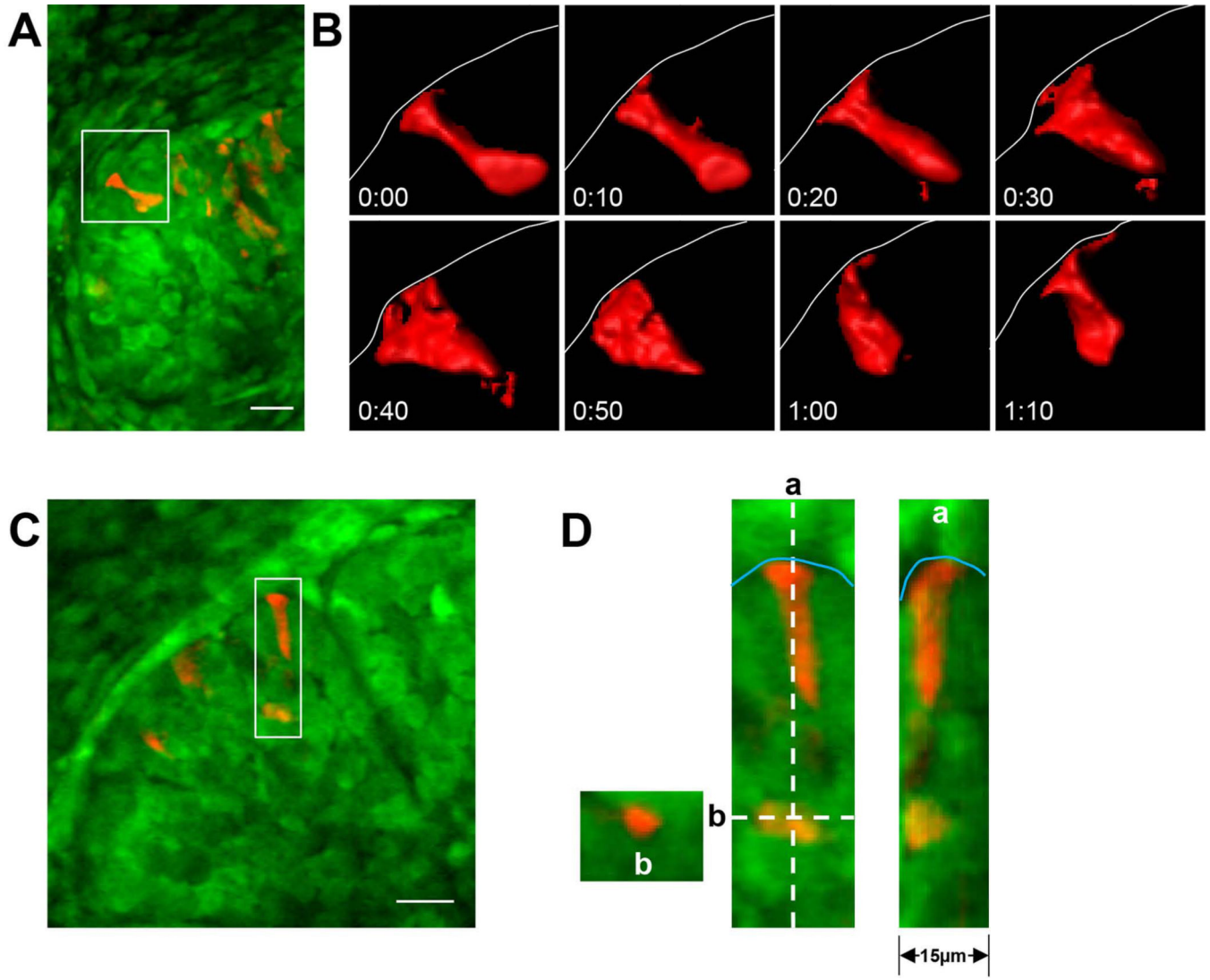

Fig. 3.

Pleomorphic shape changes of outer bud epithelial cells. **A:** Low-magnification view of KikGR-expressing cells in a submandibular gland; mesenchyme cells are at the top and left of this image, with a number of KikGR-highlighted cells in red within the epithelium. **B:** Higher-magnification view of the cell marked by the white box in panel A, shown at 10-minute intervals after isosurfacing. Note the substantial changes in cell shape while maintaining leading-edge contact as the cell interacts with the basement membrane (thin white line). **C:** and **D:** Examples of different epithelial cell shapes. The insets in D show two cells, one elongated and contacting the basement membrane (thin cyan line) and one at the border of the inner bud region. **a** and **b** show orthogonal views of each cell in the Z dimension at the respective dotted lines indicated in D. Images in A, C, and D are maximum intensity Z projections of 20 μm. Bars, 20 μm.

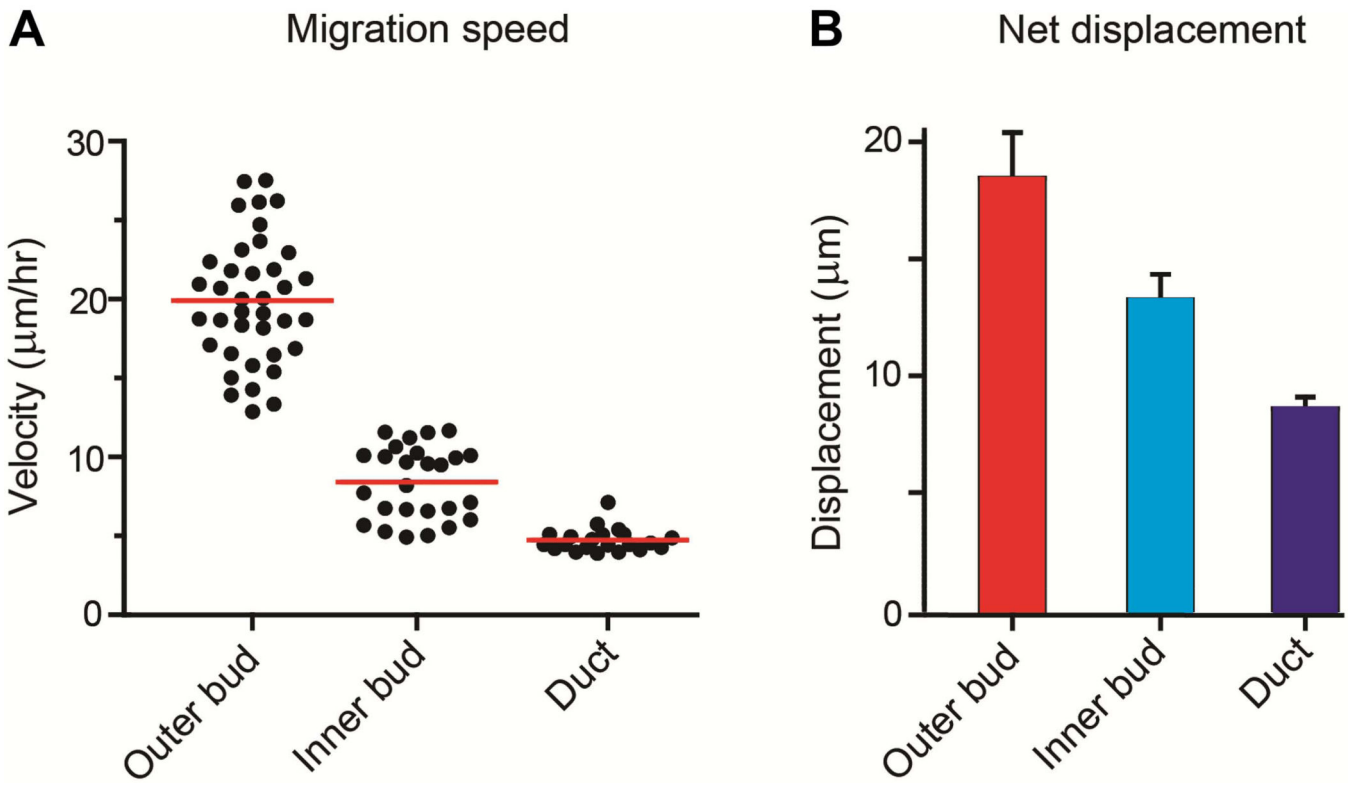

Fig. 4.

Comparison of velocities and net displacement of salivary gland epithelial cells at different locations in glands undergoing branching morphogenesis. **A:** Scatterplot analysis of all data points from untreated control glands, comparing migration velocities of outer bud cells, inner bud cells, and duct cells. According to non-parametric ANOVA analysis with Kruskal-Wallis post-test, $p<0.0001$ for outer vs. inner, outer vs. duct, and inner vs. duct cells. **B:** Bar graphs of net displacement from start to finish of automated tracking for all control outer bud, inner bud, and duct cells (160 min); $p<0.05$ for outer vs. inner bud cells, $p<0.0001$ for outer bud vs. duct cells, and $P = 0.011$ for inner bud vs. duct cells.

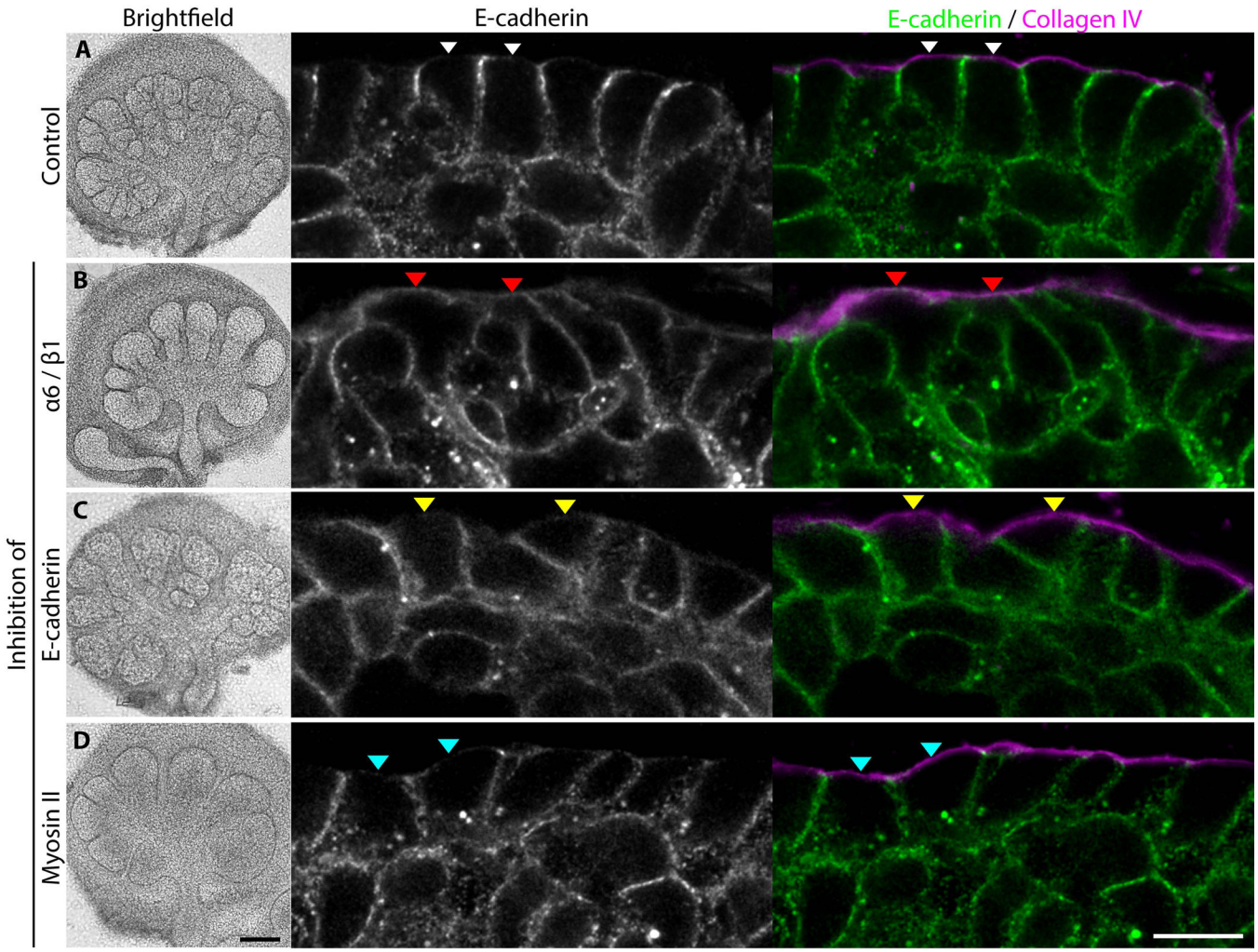

Fig. 5.

Morphological alterations resulting from inhibition of integrins, E-cadherin, or myosin II during branching morphogenesis. Submandibular glands from E14 embryos treated with **A:** no inhibitor, **B:** a mixture of 100 μg/ml each of anti-β1 antibody Ha2/5 and anti-α6 antibody GoH3, **C:** 50 μM blebbistatin, or **D:** 100 μg/ml ECCD-1 inhibitory anti-E-cadherin monoclonal antibody. Whole glands were immunostained with polyclonal goat anti-collagen IV antibody at 2 μg/ml and monoclonal antibody ECCD-2 against E-cadherin at 5 μg/ml. Each image is a single scanning confocal microscope slice. Arrowheads (A, white; B, red; C, yellow; D, cyan) highlight examples of basal plasma membrane regions associated with basement membrane. All immunostaining images are single Z-slices taken at the Z midpoint of the gland. Black bar, 200 μm; white bar, 10 μm.

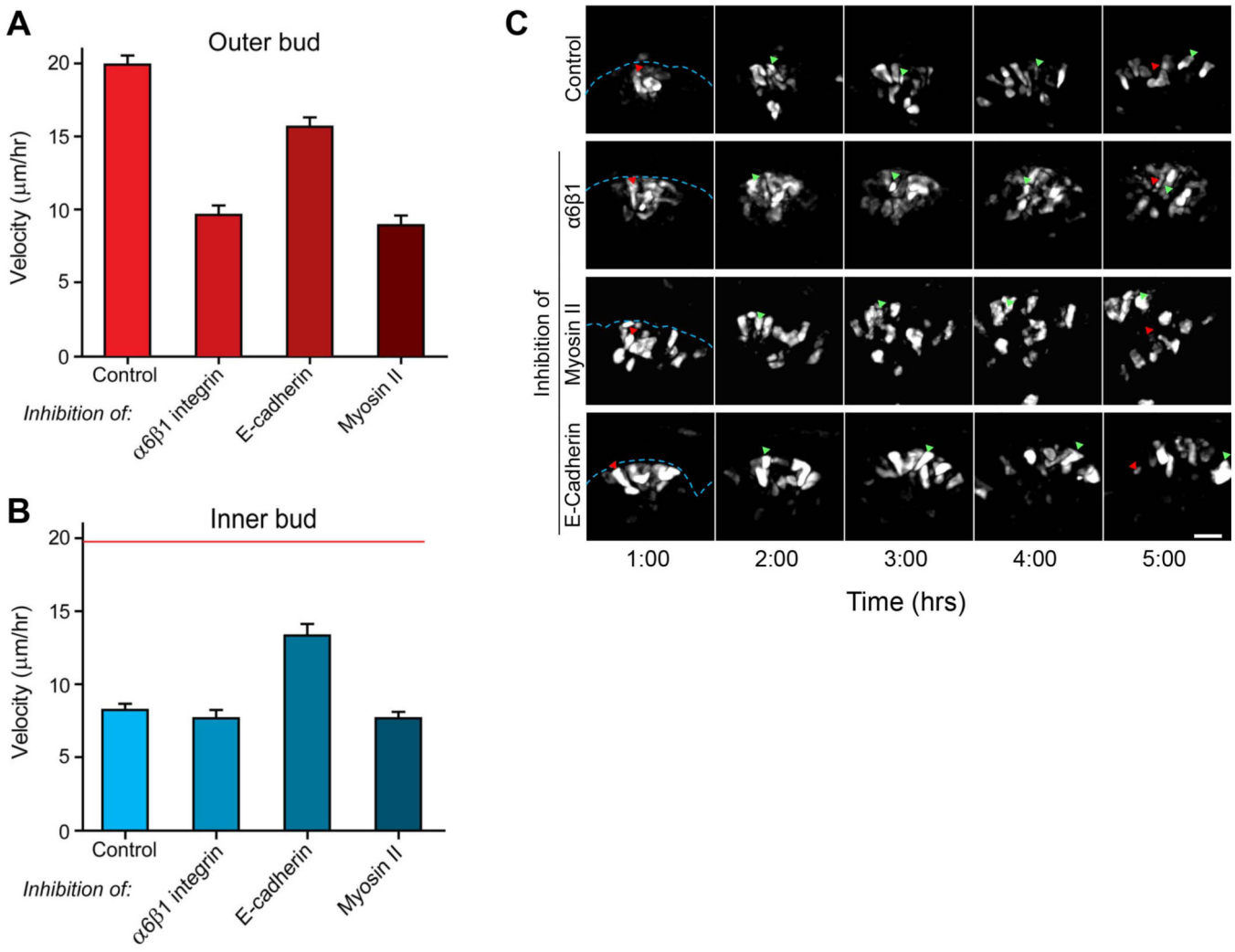

Fig. 6.

Velocities of cell migration determined by quantitative 3D tracking. **A:** Rates of cell migration velocity of outer bud cells in control glands compared to glands treated with a combination of anti-α6 and anti-β1 integrin monoclonal antibodies (100 μg/ml each), anti-E-cadherin function-blocking antibody (100 μg/ml), or 50 μM blebbistatin to inhibit non-muscle myosin II isoforms. **B:** Rates of cell migration velocity of inner bud cells in the same comparisons of inhibitors shown in panel A; for comparison, red line indicates average velocity of control outer bud cells. **C:** A 4-hour time-lapse sequence illustrating the movement of outer buds cells in an untreated control compared to the inhibitor-treated conditions described in panel A. Red arrowheads indicate the original position of a cell 1 hour after photoconversion, while the green arrowheads show its position at the indicated times. Blue dashed lines indicate the position of the basement membrane. These images are maximum intensity Z projections of 20 μm. Bar, 20 μm.

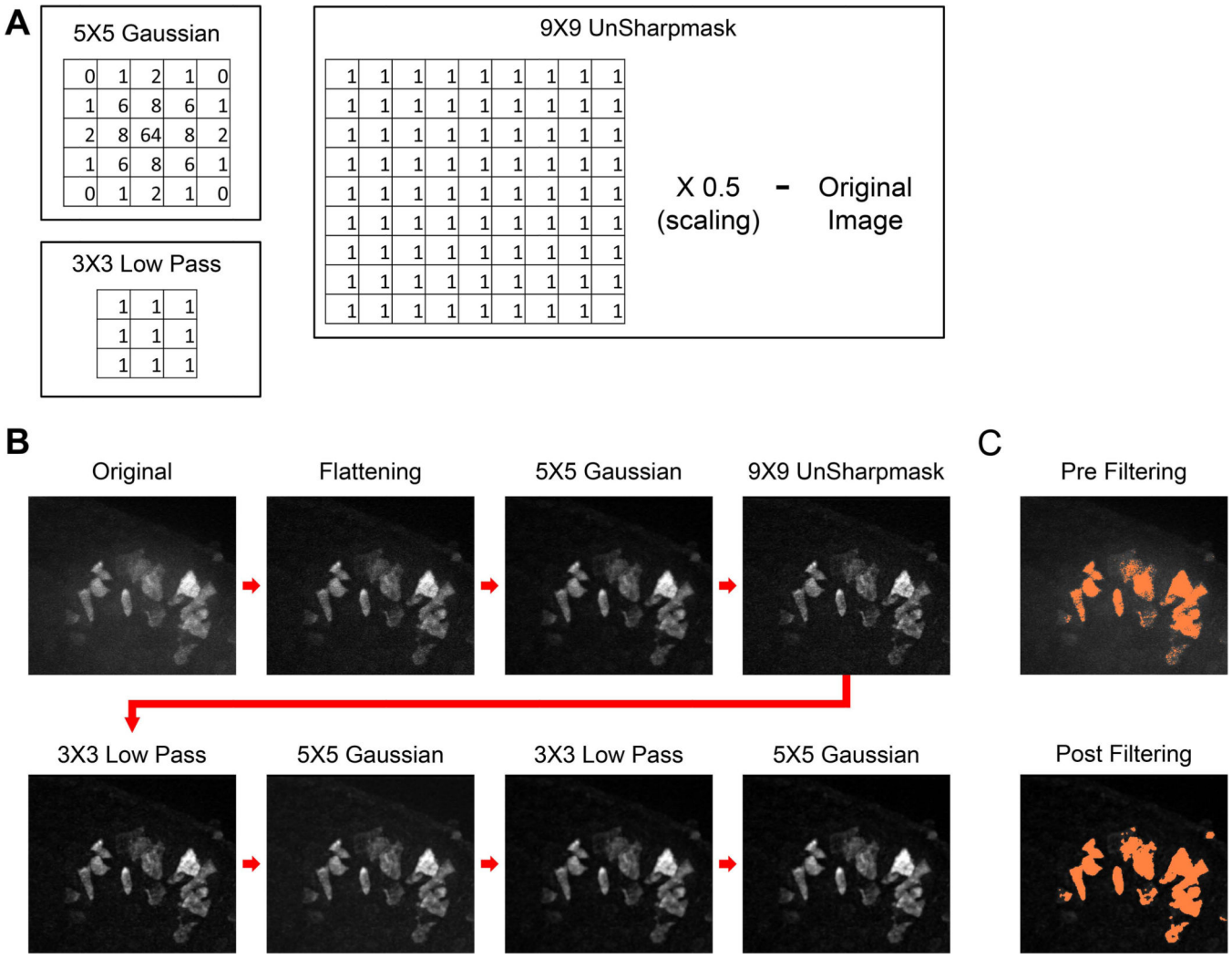

Fig. 7.

Image filter processing methods used to track 3D cell migration. **A:** Examples of filtering kernels for the 5×5 Gaussian, 3×3 low pass, and the 9×9 unsharp mask used for filtering images prior to cell tracking. For the unsharp mask, the 9×9 low pass filter was first applied to the original image, then the grayscale intensity was scaled down by half. The resulting image was then subtracted from the original image. **B:** A series of maximum-projected Z-stacks showing the image filtering sequence starting from the original image (far upper left) to the final image used for cell tracking (far lower right). **C:** Pre-filtered original shown in panel B and the final image after filtering that was masked or thresholded one standard deviation above the mean intensity. See Experimental Procedures for additional details.